High-energy bremsstrahlung from polarized electrons colliding with spin-$\frac{1}{2}$ nuclei

D. H. Jakubassa-Amundsen
Mathematics Institute, University of Munich, Theresienstrasse 39, 80333 Munich, Germany
(Received 22 February 2013; revised manuscript received 12 April 2013; published 18 June 2013)

The Born theory for bremsstrahlung from high-energy electrons colliding with extended (finite-mass) nuclei is reexamined. Higher-order effects are included into the Born approximation by making use of the weak-potential Sommerfeld-Maue prescription in an additional contribution to the transition amplitude. Predictions are made for the differential cross section (with respect to the photon degrees of freedom) and for the polarization correlations between the incoming electron and the emitted photon. It is found that at collision energies exceeding 20 MeV the cross section as well as the polarization correlations are strongly influenced by nuclear recoil and nuclear structure effects, particularly at backward photon angles. Numerical results are presented for bremsstrahlung from 10–100 MeV electrons colliding with protons, ^{19}F and ^{89}Y nuclei.

DOI: 10.1103/PhysRevC.87.064609 PACS number(s): 25.30.−c, 24.70.+s, 34.80.Pa, 41.60.−m

I. INTRODUCTION

The investigation of polarization effects in high-energy bremsstrahlung during an electron-nucleus encounter is a sensitive tool to gain supplementary information on QED effects and on the nuclear structure. If only scattering *cross sections* are considered, the electric contribution, resulting from the charge interaction between electron and nucleus, adds incoherently to the magnetic contribution which is due to the particle current interaction between the collision partners. The polarization correlations, on the other hand, are influenced by the *interference* effects between electric and magnetic scattering. Thus the relativistic and nuclear structure effects will be more easily seen in polarization measurements than in mere intensity measurements.

The study of the bremsstrahlung polarization correlations from *low-energy* electron scattering has a long tradition (highlighted by the seminal works of Tseng and Pratt [1] on the theory side and of Nakel and collaborators [2] on the experimental side). This subject has recently been taken up in a series of experimental investigations [3–7] at collision energies between 0.1–3.5 MeV. For *high-energy* electron scattering, i.e., for energies above 20 MeV, the basic subject has been the investigation of the intensity of bremsstrahlung emitted by unpolarized electrons [8]. An exception was the consideration of the spin asymmetry from the scattering of unpolarized electrons by polarized target nuclei in the GeV region [9].

The motivation for investigating high-energy bremsstrahlung has primarily been the consideration of radiative corrections to electron-nucleus scattering if only the electron or the nucleus, but not the photon, is observed [10–13]. A second topic of interest is the measurement of beam polarization during an experiment. This can be done with the help of Compton polarimetry which is based on the polarization transfer in electron-photon interactions. It is a challenge to apply this technique above electron energies of, say, 10 MeV [5], but there are strong arguments that such polarization measurements are feasible up to several tens of MeV [14,15].

Since accurate partial-wave calculations are only feasible up to at most 5–10 MeV [16–18], the lowest-order Born approximation (usually termed 'first-order' Born approximation although it is a second-order process [19]) is commonly used for collision energies extending into the nuclear physics regime. Motivated by the fact that the spin asymmetry A (for electrons spin-polarized perpendicular to the reaction plane) vanishes in the first-order Born approximation, there are—in particular for low-energy scattering—several attempts to use the second-order Born approximation. This theory is hampered by divergences in some contributions to the transition amplitude which however, can be handled to provide a finite cross section [20]. For energies below 1 MeV the second-order Born approximation was, e.g., applied to the calculation of A in [21][1] and [22].

A widely used approximation, which includes the Born series to all orders but which is restricted to weak potentials ($Z/c \ll 1$) or ultrahigh electron energies, is the Sommerfeld-Maue model (also termed Elwert-Haug theory [23]). In this theory the Dirac functions for the incoming and the scattered electron are approximated by the semirelativistic Sommerfeld-Maue wave functions [24] which allow for an analytic evaluation of the radiation matrix element [25]. The disadvantage of this theory in its application to high-energy bremsstrahlung is its formulation for point-like nuclei only.

In the nuclear physics regime there are several effects which introduce changes into the standard bremsstrahlung theories as applied for low collision energies. First, the finite mass of the nucleus has to be taken into consideration, which leads to recoil effects [11]. These recoil corrections consist of a kinematical contribution, due to the modification of the energy balance, and of a dynamical contribution (also called 'virtual Compton effect' [9]), which originates from bremsstrahlung emission by the *nucleus* [26,27]. Secondly, in addition to the charge interaction, also the magnetic scattering has to be accounted for (see, e.g., [8]). Moreover, there are modifications due to the finite nuclear size [28]. The nuclear structure effects [13,29] also cause the presence of an anomalous magnetic moment and

[1]Formula (24) of that work, claiming that A is linearly dependent on the nuclear charge Z, has to be treated with care. The approximation leading to Eq. (24) is incorrect for the larger Z, and one always has $|A| \leqslant 1$, also in a *consistent* second-order Born theory.

may even allow for resonant intermediate nuclear states [9] or the excitation of the nucleus [30].

While the high-energy bremsstrahlung calculations in the middle of last century usually suffer from several additional approximations which were made in order to reduce the computational task, nowadays computers allow for an exact evaluation of the bremsstrahlung models in question. In the present work we start from the conventional first-order Born approximation which is modified to include nuclear recoil as well as magnetic and nuclear structure effects (Sec. II). Section III provides a detailed comparison with results from the (point-nucleus) Bethe-Heitler theory for the differential cross section (integrated over the electron degrees of freedom), for the linear polarization P_1 and for the circular polarization correlation P_3 which can be calculated in the first-order Born approximation. Assuming that the sum of magnetic and recoil contributions to scattering will induce similar (mostly moderate) modifications of the higher-order correction terms, as they do for the first-order terms, we include the higher-order effects by making use of the Sommerfeld-Maue prescription for spinless point nuclei (Sec. IV). With this higher-order theory the spin asymmetry A and the polarization correlation P_2 are calculated (Sec. V). The results are summarized in Sec. VI. Atomic units ($\hbar = m = e = 1$) are used throughout. In particular, it is important to retain the electron mass m, even at ultrahigh collision energies.

II. THE BORN APPROXIMATION (PWBA) FOR STRUCTURED NUCLEI

We provide an outline of the Born theory for high-energy bremsstrahlung by generalizing the formalism for electron-electron bremsstrahlung [2,31] to the radiative interaction between a spin-polarized electron and a heavy collision partner of nuclear charge Z and spin $\frac{1}{2}$. Restriction is made to the case where only the photon, but not the scattered particles are observed.

A. The first-order transition amplitude with kinematical recoil

Consider the emission of a photon with polarization direction $\boldsymbol{e}_\lambda$ by a relativistic beam electron with total energy E_i and mass m during the encounter with a nucleus at rest (termed 'electron bremsstrahlung'). The first-order Born approximation for this process consists of two Feynman diagrams, one where the electron emits the photon after the interaction with the nucleus and the other where the two processes occur in the reversed order [Fig. 1(a)]. Let $u_{k_i}^{(\sigma_i)}$ be the free Dirac four-spinor of the electron in its initial state, described by the momentum four-vector $k_i \equiv (k_i^\nu) = (E_i/c, \boldsymbol{k}_i)$ and the spin polarization σ_i, and let $u_{k_f}^{(\sigma_f)}$ be the respective four-spinor for the final electronic state. Let $U_{P_i}^{(s_i)}$ and $U_{P_f}^{(s_f)}$ be the four-spinors describing, respectively, the initial and final states of a spin-$\frac{1}{2}$ nucleus. We have $P_i = (E_{\mathrm{nuc},i}/c, \boldsymbol{0})$ and $P_f = (E_{\mathrm{nuc},f}/c, \boldsymbol{P}_f)$, where $E_{\mathrm{nuc}} = \sqrt{\boldsymbol{P}^2c^2 + M_T^2c^4}$ is the total energy of the nucleus of mass M_T and three-momentum $\boldsymbol{P}$, and s_i and s_f are, respectively, the nuclear spin projections. In the notation of Bjorken and Drell [32] the transition amplitude relating to these two diagrams is given by [29,31]

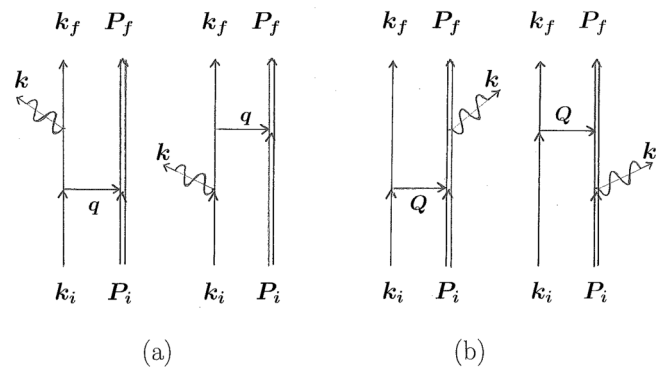

FIG. 1. Feynman diagrams (a) for electron bremsstrahlung, (b) for nucleus bremsstrahlung. The respective momentum transfer to the nucleus is denoted by $\boldsymbol{q}$ and $\boldsymbol{Q}$.

$$A_{fi}^{\mathrm{el}} = \frac{1}{q^2}\sum_{\nu=0}^{3}\left(u_{k_f}^{(\sigma_f)+}\left[(\boldsymbol{\alpha}\boldsymbol{e}_\lambda^*)\frac{1}{\not{k}_f + \not{k} - m}\gamma^\nu + \gamma_0\gamma^\nu\frac{1}{\not{k}_i - \not{k} - m}\gamma_0(\boldsymbol{\alpha}\boldsymbol{e}_\lambda^*)\right]u_{k_i}^{(\sigma_i)}\right) \times \frac{Z}{2\pi^2c^2}\left(U_{P_f}^{(s_f)+}\gamma_0\Gamma_\nu(q)U_{P_i}^{(s_i)}\right), \tag{2.1}$$

where $k = (\omega/c, \boldsymbol{k})$, with $\omega = |\boldsymbol{k}|c$, is the four-momentum of the emitted photon. In Eq. (2.1) the following abbreviation is used:

$$\frac{1}{\not{p} \pm \not{k} - m} = -\frac{\boldsymbol{\alpha}c(\boldsymbol{p} \pm \boldsymbol{k}) + \beta mc^2 + (E_p \pm \omega)}{(\boldsymbol{p} \pm \boldsymbol{k})^2 - \left(\left(\frac{E_p \pm \omega}{c}\right)^2 - m^2c^2\right)}\gamma_0, \qquad E_p = \sqrt{\boldsymbol{p}^2c^2 + m^2c^4}. \tag{2.2}$$

$q = P_f - P_i = (q_0, \boldsymbol{q})$ is the four-momentum transfer, with $q^2 = (E_{\mathrm{nuc},f}/c - E_{\mathrm{nuc},i}/c)^2 - \boldsymbol{P}_f^2$, and $\Gamma_\nu(q)$ accounts for the nuclear structure and anomalous magnetic moment effects by means of [32–34][2]

$$\gamma_0\Gamma_\nu(q) = F_1(q)\begin{Bmatrix}1\\-\alpha_l\end{Bmatrix} + \frac{\kappa}{2M_pcZ}F_2(q) \times \begin{cases}\gamma_0\boldsymbol{q}\boldsymbol{\alpha}, & \nu = 0\\ \gamma_0 M_l(q), & \nu = l = 1, 2, 3,\end{cases} \tag{2.3}$$

where γ^ν, β and $\boldsymbol{\alpha} = (\alpha_1, \alpha_2, \alpha_3)$ are Dirac matrices, $M_l(q) = -\alpha_l q_0 + i(\boldsymbol{q} \times \boldsymbol{\Sigma})_l$ with $\Sigma_l = \left(\begin{smallmatrix}\sigma_l & 0\\ 0 & \sigma_l\end{smallmatrix}\right)$, and where $\boldsymbol{\sigma} = (\sigma_1, \sigma_2, \sigma_3)$ is the vector of Pauli spin matrices. F_1 and F_2 are, respectively, the Dirac and Pauli form factors, and κ is the anomalous magnetic moment in units of the Bohr magneton (with M_p the proton mass).

From the conservation of the four-momentum,

$$P_f = k_i + P_i - k_f - k, \tag{2.4}$$

one obtains, upon squaring both sides of Eq. (2.4) (following [2] by using $k_i^2 = k_f^2 = m^2c^2$, $P_i^2 = P_f^2 = M_T^2c^2$, $k^2 = 0$), a

[2] In Eq. (2.6) of [34] M_pc should be replaced by M_pc^2 since in that work q is of dimension [energy].

quadratic equation for the final electron momentum $|\boldsymbol{k}_f|$ with the solution

$$|\boldsymbol{k}_f| = \frac{1}{f_1^2c^2 - f_2^2}\left(af_2 + f_1c\sqrt{a^2 + f_2^2c^2 - f_1^2c^4}\right),$$
$$a = c^2 + E_i(M_T - |\boldsymbol{k}|/c) - M_T|\boldsymbol{k}|c + \boldsymbol{k}_i\boldsymbol{k}, \qquad (2.5)$$
$$f_1 = E_i/c^2 + M_T - |\boldsymbol{k}|/c, \quad f_2 = \hat{\boldsymbol{k}}_f(\boldsymbol{k}_i - \boldsymbol{k}).$$

Note that $|\boldsymbol{k}_f|$ depends on the unit vector $\hat{\boldsymbol{k}}_f$ in the direction of the scattered electron [11]. In the limit $M_T \to \infty$, the low-energy relation $E_f \equiv E_{f\infty} = E_i - \omega$ is recovered instead.

A consequence of taking the energy transfer to the nucleus into consideration is the termination of the bremsstrahlung spectrum at a frequency $\omega_{\max}$ which can be considerably smaller than the low-energy short-wavelength limit $\omega_{\rm SWL} = E_i - mc^2$. The fact that $\omega_{\max}$ is not fixed but depends on the photon angle θ_k is well known from electron-electron bremsstrahlung [2]. Generalizing the respective formula to the case of electron-nucleus collisions, $\omega_{\max}$ is found from

$$\omega_{\max} = |\boldsymbol{k}_{\max}|c = \frac{M_Tc^2(E_i - c^2)}{E_i - |\boldsymbol{k}_i|c\cos\theta_k + M_Tc^2}. \qquad (2.6)$$

At large E_i ($E_i \approx |\boldsymbol{k}_i|c$), one has approximately $\omega_{\max} \approx E_i/(1 + \frac{E_i}{M_Tc^2}(1 - \cos\theta_k))$.

B. The dynamical recoil

Since the nucleus has nonzero momentum $\boldsymbol{P}_f$ after the collision, it will also contribute to the photon emission. However, the amplitude for this 'nuclear bremsstrahlung' is in general reduced by a factor qZ/M_Tc [26]. Again, two Feynman diagrams have to be considered for this process [Fig. 1(b)], including the one where the photon is emitted prior to the electron-nucleus encounter [26,27]. The corresponding transition amplitude is given by [29]

$$A_{fi}^{\rm nuc} = -\frac{Z}{Q^2}\sum_{\nu=0}^{3}\left(u_{k_f}^{(\sigma_f)+}\gamma_0\gamma^\nu u_{k_i}^{(\sigma_i)}\right)$$
$$\times\left(U_{P_f}^{(s_f)+}\left[\gamma_0\not{E}\frac{1}{\not{P}_f + \not{k} - M_T}\Gamma_\nu(Q)\right.\right.$$
$$\left.\left. + \gamma_0\Gamma_\nu(Q)\frac{1}{\not{P}_i - \not{k} - M_T}\not{E}\right]U_{P_i}^{(s_i)}\right) \times \frac{Z}{2\pi^2c^2}, \qquad (2.7)$$

where $Q = k_i - k_f$ is the respective momentum transfer. The emission of the photon is also influenced by the nuclear structure effects, hence $\boldsymbol{\alpha}\boldsymbol{e}_\lambda^*$ is replaced by $\gamma_0\not{E}$ with

$$\not{E} = \boldsymbol{\Gamma}(K)\boldsymbol{e}_\lambda^*, \quad \boldsymbol{\Gamma}(K) = (\Gamma^l(K)) = -(\Gamma_l(K)). \qquad (2.8)$$

The argument $K = (K_0, \boldsymbol{K})$ in the matrix Γ_l from Eq. (2.3) relates to an outgoing photon the momentum of which is directed *away* from the nuclear line in the Feynman diagrams, in contrast to the virtual photons represented by $\boldsymbol{q}$ or $\boldsymbol{Q}$. The argument of Γ_l for an outgoing photon can be determined from the fact that Γ_l has to behave like γ_l under time reversal, or equivalently, under complex conjugation. With ${\gamma_l}^+ = -\gamma_l$ and $(\gamma_0\alpha_l)^+ = \alpha_l\gamma_0 = -\gamma_0\alpha_l$ it follows from $\Gamma_l(K)^+ = -\Gamma_l(k)$ that $K = (-\omega/c, \boldsymbol{k})$ for a photon with four-momentum k. The form factors $F_1(K)$ and $F_2(K)$ entering into $\Gamma_l(K)$ only depend on the modulus of K [32]. Since $K^2 = 0$ and $F_1(0) = F_2(0) = 1$, the form factors can be disregarded.

C. The differential cross section and the polarization correlations

We restrict ourselves to a scenario where the nucleus is initially unpolarized. Since neither the outgoing electron nor the recoiling nucleus are observed, we have to average over the initial nuclear spin s_i and to sum over the final spins s_f and σ_f. In addition we have to integrate over the energy and the solid angle $d\Omega_f$ of the scattered electron. The doubly differential cross section for the emission of a photon with frequency ω and polarization direction $\boldsymbol{e}_\lambda$ into the solid angle $d\Omega_k$ is obtained from [2,34,35]

$$\frac{d^2\sigma}{d\omega d\Omega_k}(\boldsymbol{\zeta}_i, \boldsymbol{e}_\lambda) = \frac{4\pi^2\omega}{c^3v}\left(\frac{m}{2M_Tc^2}\right)^2\frac{1}{2}\sum_{s_i}\sum_{s_f,\sigma_f}\int d\Omega_f$$
$$\times\frac{|\boldsymbol{k}_f|E_f}{f_{re}}\left|A_{fi}^{\rm el} + A_{fi}^{\rm nuc}\right|^2, \qquad (2.9)$$

with v the collision velocity and $A_{fi}^{\rm el}$ and $A_{fi}^{\rm nuc}$ the amplitudes from, respectively, Eqs. (2.1) and (2.7). The recoil factor f_{re} originates from the integration over the momentum $|\boldsymbol{k}_f|$ of the electron [2,28],

$$\int_0^\infty \boldsymbol{k}_f^2 d|\boldsymbol{k}_f|\delta(E_i + E_{{\rm nuc},i} - E_f - E_{{\rm nuc},f} - \omega)$$
$$= \frac{\boldsymbol{k}_f^2}{\frac{d}{d|\boldsymbol{k}_f|}(E_f + E_{{\rm nuc},f})}, \qquad (2.10)$$

using that $E_{{\rm nuc},f} = \sqrt{\boldsymbol{P}_f^2c^2 + M_T^2c^4}$ with P_f from Eq. (2.4). Thus, when compared to the case $\boldsymbol{P}_f = \boldsymbol{0}$, one obtains

$$f_{re} = 1 - \frac{\hat{\boldsymbol{k}}_f\boldsymbol{q}E_f}{|\boldsymbol{k}_f|E_{{\rm nuc},f}}. \qquad (2.11)$$

The prefactor $(m/2M_Tc^2)^2$ in Eq. (2.9) arises from the normalization of the nuclear free four-spinors to $2M_Tc^2$ [33]. $\boldsymbol{\zeta}_i$ denotes the spin vector of the beam electron, and the corresponding spinor is given by

$$u_{k_i}^{(\sigma_i)} = e^{-i\varphi_s/2}\cos\frac{\alpha_s}{2}u_{k_i}^{(+)} + e^{i\varphi_s/2}\sin\frac{\alpha_s}{2}u_{k_i}^{(-)}, \qquad (2.12)$$

with the basis vectors $u_{k_i}^{(\pm)}$ (describing electron spins aligned with $\boldsymbol{k}_i$) defined by

$$u_{k_i}^{(\pm)} = \sqrt{\frac{E_i + c^2}{2E_i}}\begin{pmatrix}1\\ \frac{\boldsymbol{\sigma}\boldsymbol{k}_ic}{E_i + c^2}\end{pmatrix}\chi_{\pm\frac{1}{2}},$$
$$\chi_{\frac{1}{2}} = \begin{pmatrix}1\\0\end{pmatrix}, \quad \chi_{-\frac{1}{2}} = \begin{pmatrix}0\\1\end{pmatrix}, \qquad (2.13)$$

and where α_s and φ_s are, respectively, the polar and azimuthal angles of $\boldsymbol{\zeta}_i$.

There are seven independent polarization correlations between $\boldsymbol{\zeta}_i$ and $\boldsymbol{e}_\lambda$, originally classified by Tseng and Pratt [1]. One can distinguish between those which are related to a linearly or to a circularly polarized photon. A linearly polarized

photon is characterized by

$$\boldsymbol{e}_\lambda = \sin\varphi_\lambda \boldsymbol{e}_{\lambda_1} + \cos\varphi_\lambda \boldsymbol{e}_{\lambda_2}, \quad \varphi_\lambda \in [0,\pi),$$
$$\boldsymbol{e}_{\lambda_1} = \begin{pmatrix} 0 \\ 1 \\ 0 \end{pmatrix}, \quad \boldsymbol{e}_{\lambda_2} = \begin{pmatrix} -\cos\theta_k \\ 0 \\ \sin\theta_k \end{pmatrix}, \tag{2.14}$$

where a coordinate system has been chosen with the z-axis along $\boldsymbol{k}_i$, the y-axis normal to the reaction plane, i.e., along $\boldsymbol{k}_i \times \boldsymbol{k}$ [where $\boldsymbol{k} = \frac{\omega}{c}(\sin\theta_k, 0, \cos\theta_k)$], and the x-axis along $\boldsymbol{e}_y \times \boldsymbol{k}_i$. The polarization correlations P_1 and P_2 (also termed Stokes parameters [36]) are defined by ($d\sigma$ abbreviating $d^2\sigma/d\omega d\Omega_k$)

$$P = \frac{d\sigma(\boldsymbol{\zeta}_i, \boldsymbol{e}_\lambda(\varphi_\lambda)) - d\sigma(\boldsymbol{\zeta}_i, \boldsymbol{e}_\lambda(\varphi_\lambda + \pi/2))}{d\sigma(\boldsymbol{\zeta}_i, \boldsymbol{e}_\lambda(\varphi_\lambda)) + d\sigma(\boldsymbol{\zeta}_i, \boldsymbol{e}_\lambda(\varphi_\lambda + \pi/2))}, \tag{2.15}$$

where for in-plane electron spin polarization (i.e., $\varphi_s = 0$) $P = P_1$ (independent of α_s) if $\varphi_\lambda = 0$ and $P = P_2(\alpha_s) = -C_{31}\cos\alpha_s + C_{11}\sin\alpha_s$ if $\varphi_\lambda = \pi/4$. P_2 is thus described by two parameters, $C_{31} = -P_2(0)$ and $C_{11} = P_2(90^\circ)$ (see also [37]).

Circularly polarized photons, i.e., photons in helicity eigenstates, are characterized by

$$\boldsymbol{e}^*_\pm = \frac{1}{\sqrt{2}}\left(\boldsymbol{e}_{\lambda_2} \pm i\boldsymbol{e}_{\lambda_1}\right), \tag{2.16}$$

where the upper sign (respectively, the lower sign) denotes right- (respectively left-)circularly polarized photons. The polarization correlation P_3 is defined for $\varphi_s = 0$ by [36,38]

$$P_3(\boldsymbol{\alpha}_s) = \frac{d\sigma(\boldsymbol{\zeta}_i, \boldsymbol{e}_+) - d\sigma(\boldsymbol{\zeta}_i, \boldsymbol{e}_-)}{d\sigma(\boldsymbol{\zeta}_i, \boldsymbol{e}_+) + d\sigma(\boldsymbol{\zeta}_i, \boldsymbol{e}_-)} = C_{32}\cos\alpha_s - C_{12}\sin\alpha_s, \tag{2.17}$$

and is also characterized by two parameters, $C_{32} = P_3(0)$ and $C_{12} = -P_3(90^\circ)$. The spin asymmetry A requires $\boldsymbol{\zeta}_i$ to be perpendicular to the scattering plane (i.e., $\alpha_s = \pi/2, \varphi_s = -\pi/2$) and is calculated from

$$A = \frac{\sum_\lambda (d\sigma(\boldsymbol{\zeta}_i, \boldsymbol{e}_\lambda) - d\sigma(-\boldsymbol{\zeta}_i, \boldsymbol{e}_\lambda))}{\sum_\lambda (d\sigma(\boldsymbol{\zeta}_i, \boldsymbol{e}_\lambda) + d\sigma(-\boldsymbol{\zeta}_i, \boldsymbol{e}_\lambda))}, \tag{2.18}$$

where $\sum_\lambda$ denotes the sum over the two photon polarizations. Note that A is independent of the chosen representation of $\boldsymbol{e}_\lambda$.

III. NUMERICAL RESULTS WITHIN THE BORN APPROXIMATION

Let us start with providing results for the bremsstrahlung cross sections and for the polarization correlations P_1 and P_3 which can be calculated within the plane-wave Born approximation (PWBA). For the Born theory to be applicable, restriction is made to nuclei where Z/c is small. The validity of the Born approximation can be verified by comparing the results from the Bethe-Heitler (BH) theory (see, e.g., [2,19] and Sec. IV) with those from the Sommerfeld-Maue (SM) theory. For protons the Born approximation is excellent, and it works also well for the ^{19}F nucleus (see, e.g., [1]). In particular, the cross sections agree in general within 1% except at photon frequencies near $\omega_{\rm SWL}$, since the BH cross section tends to zero at the short-wavelength limit (while it remains finite in the SM theory). For the heaviest nucleus considered, ^{89}Y, the deviations between the BH and SM theory are well below 20%, except at the back-most photon angles if the ratio R between the photon frequency and the beam energy gets close to unity. For example, when $R = 0.5$, no restriction on the angle θ_k is necessary, while for $R = 0.8$, the deviations will exceed 20% if $\theta_k \gtrsim 160^\circ$.

For the specification of the form factors we assume a spherically symmetric charge distribution $\varrho(r)$, which is generally the case for spin $\frac{1}{2}$ nuclei. For moderate momentum transfers q the electric form factor $G_E(q)$ (also identified with $F_L(q)(1 + q^2/4M_T^2c^2)^{-1/2}$, see, e.g., [39]) can be approximated by the Fourier transform

$$G_E(q) = \frac{4\pi}{Z}\int_0^\infty r^2 dr \varrho(r) j_0(\tilde{q}r), \tag{3.1}$$

where j_0 is a spherical Bessel function and $\tilde{q} = \sqrt{-q^2}$. $\varrho(r)$, normalized to Z, can be taken from [40] for protons and from the tables of [41] for the heavier nuclei. Fermi charge distributions are used with parameters $c_0 = 2.58$ fm and $a = 0.567$ fm for ^{19}F and $c_0 = 4.76$ fm and $a = 0.571$ fm for ^{89}Y.

The experimental magnetic moments of the three nuclei are $\mu_{\rm exp} = 2.79$ for protons, 2.629 for ^{19}F and -0.13742 for ^{89}Y [42], defining $\kappa = \mu_{\rm exp} - \frac{M_p}{M_T}$. The magnetic form factor $G_M(q)$ (also identified with $\frac{\sqrt{2}M_pc}{\tilde{q}}F_T(q)$ [39,43]) for ^{1}H and ^{19}F is extracted from the literature [40,43] as described in [34].

For the ^{89}Y nucleus the relation between $G_M(q)$ and the $M1$ magnetization current density $J_{11}(r)$ is used (in [44], $F_L \equiv F^C$, $F_T \equiv F^M$),

$$G_M(q) = \frac{N_0}{\tilde{q}}\int_0^\infty r^2 dr J_{11}(r) j_1(\tilde{q}r). \tag{3.2}$$

From the linear behavior of the spherical Bessel function $j_1(x)$ as $x \to 0$ [viz. $j_1(\tilde{q}r)/\tilde{q}r \to \frac{1}{3}$] and from the normalization $G_M(0) = \mu_{\rm exp}$ [33], the constant N_0 can be obtained, $N_0 = 3\mu_{\rm exp}(\int_0^\infty J_{11}(r)r^3dr)^{-1}$. $J_{11}(r)$ is taken from a fit to experiment as plotted in [44]. From Eqs. (3.1) and (3.2) the Dirac and Pauli form factors are obtained by means of [32,34,43]

$$F_1(q) = \left(G_E(q) - \frac{q^2}{4M_pM_Tc^2}G_M(q)\right)\Big/\left(1 - \frac{q^2}{4M_T^2c^2}\right)$$
$$F_2(q) = \left(G_M(q) - \frac{M_p}{M_T}F_1(q)\right)\Big/\kappa. \tag{3.3}$$

For the separate study of recoil and magnetic effects the form factors as well as the anomalous magnetic moment can be switched off in the transition amplitudes $A_{fi}^{\rm el}$ and $A_{fi}^{\rm nuc}$, and the corresponding model will be referred to as BRM theory. If, in addition, the dynamical recoil and the magnetic interaction is also switched off (so that only the kinematical recoil with $\nu = 0$ is retained), the model will be called BR0 theory. For a compilation of the models, see Table I.

TABLE I. Theoretical models for bremsstrahlung calculations. BR0 and BRM are only auxiliary models to demonstrate the importance of recoil and magnetic scattering.

Models	Ingredients
BH	Plane-wave Born; fixed point nucleus
BR0	Plane-wave Born; point nucleus, kinematical recoil
BRM	Plane-wave Born; point nucleus, total recoil, magnetic scattering
PWBA	Plane-wave Born; extended nucleus, total recoil, magnetic scattering
SM	Higher-order, semirelativistic functions; fixed point nucleus
WPA	Higher-order, semirelativistic functions; extended nucleus, total recoil, magnetic scattering in plane-wave Born

These different models are investigated for protons, the case most extensively discussed in the literature. Figure 2(a) shows the angular dependence of the bremsstrahlung cross section for a beam energy $E_{i,\mathrm{kin}} = E_i - c^2 = 50$ MeV and for the ratio $R = \omega/E_{i,\mathrm{kin}} = 0.5$. It is seen that the Bethe-Heitler theory performs very well up to photon angles near 120°. The inclusion of the kinematical recoil (as considered in the BR0 theory) leads to a slight decrease of the cross section at the back-most angles, while the inclusion of the magnetic effects (via the BRM theory) overcompensates this decrease. The consideration of the anomalous magnetic moment (in the PWBA) leads to a further increase (whereas the momentum transfer is still too small to cause a noticeable decrease of the proton form factors).

In the early papers the recoil effects were genuinely disregarded, with reference to the work by Drell [26] for collision energies up to 200 MeV. Drell did consider the dynamical recoil, but restricting himself to the potential contribution [i.e., setting $\nu = 0$ in Eqs. (2.1) and (2.7)] and to photons emitted close to the beam direction, he found that recoil does not affect the cross section. This is, however, no longer true for wide-angle bremsstrahlung. As demonstrated in Fig. 2(a), the $\nu = 0$ approximation (with dynamical recoil included) is incorrect and recoil becomes increasingly important with increasing photon angle. In fact, there is a significant cancellation between the recoil affecting the potential scattering and the recoil affecting the magnetic scattering, with the BRM results being again close to the BH results.

In the linear polarization P_1 the influence of recoil effects and magnetic scattering is much larger (the $\nu = 0$ approximation including dynamical recoil would even lead to large *positive* values of P_1 beyond 60°). From Fig. 2(b) it follows that the BH theory fails already in the forward hemisphere, and that the PWBA leads to a strong enhancement of P_1 in the angular region 60°–150°. At very small angles (below 10°), corresponding to electron-nucleus distances much larger than the nuclear charge distribution, all theories coincide. As known from earlier investigations above 1 MeV [17,37,45], P_1 has a forward maximum for a ratio R close to 1, which decreases in height and is shifted to smaller θ_k as E_i increases. When R gets smaller or E_i is sufficiently high, a forward minimum develops which, for the parameters of Fig. 2(b), lies at $\theta_k = 0.6°$ and has a value of -0.44 (suppressed in the figure). Note that $P_1 = 0$ at 0° and 180° where the reaction plane collapses to a line.

The dependence on ω for fixed beam energy is displayed in Fig. 3 at the two photon angles 100° and 170°. From Fig. 3(a) it is seen that the sensitivity of the cross section to the relativistic nuclear effects increases with ω. Also displayed is the reduction of the short-wavelength limit as compared to the BH theory, which is the more pronounced the larger the photon angle. In Fig. 3(b) one can trace the transition of an increase of P_1 near the short-wavelength limit in the BH theory to a decrease of P_1 in the PWBA by successively including the kinematical recoil (BR0 theory), the dynamic recoil and the Dirac magnetic moment (BRM theory) and finally the nuclear structure effects (PWBA).

In Fig. 4 it is shown how the magnetic and the nuclear structure effects come into play at backward angles when the collision energy is increased, while the photon angle and the ratio R are kept fixed. A comparison between the BH theory and the PWBA shows that for protons these effects lead to

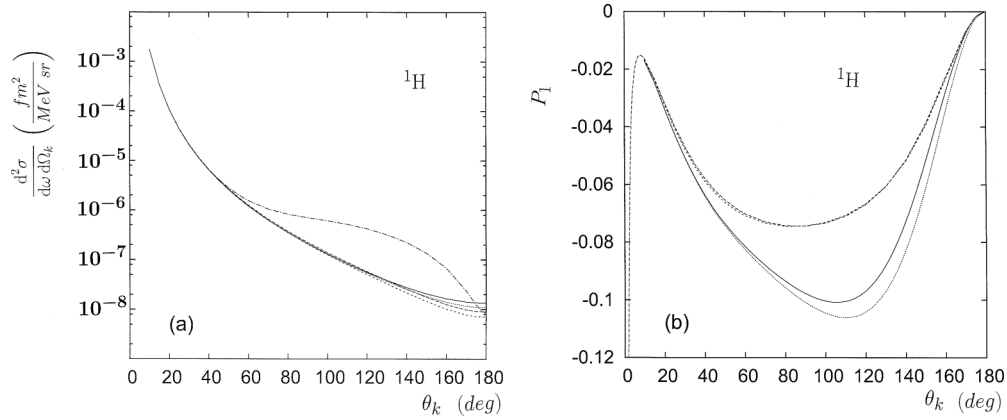

FIG. 2. (a) Doubly differential cross section and (b) linear polarization P_1 for 50 MeV $e + p$ collisions with photon emission at $\omega = 25$ MeV as a function of photon angle θ_k. Solid line, PWBA; dotted line, BRM theory; long-dashed line, BH theory; short-dashed line, BR0 theory [lowermost curve in (a), second curve from top in (b)]; dash-dotted line, $\nu = 0$ but with dynamical recoil included. (1 fm^2/MeV sr $= 10^{-5}$ b/keV sr.)

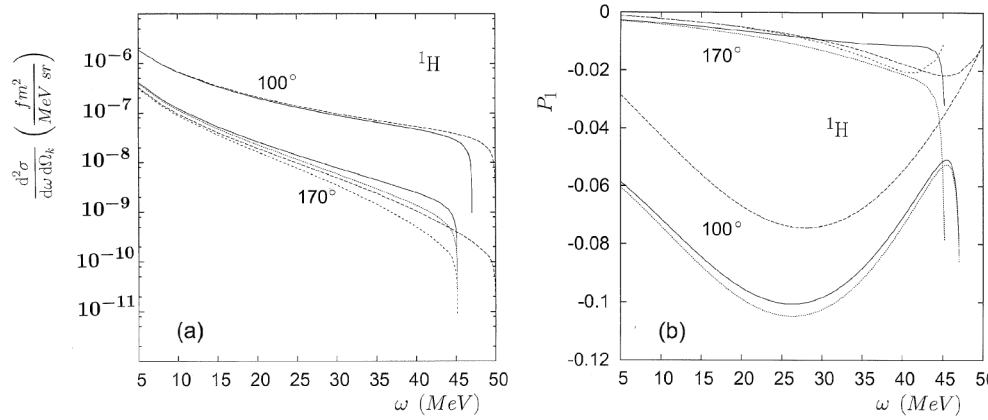

FIG. 3. (a) Doubly differential cross section and (b) linear polarization for 50 MeV $e + p$ collisions as a function of frequency ω of the emitted photon. The upper curves in (a) and the three lower curves in (b) are for photon angle $\theta_k = 100°$, the lower curves in (a) and the upper curves in (b) are for $\theta_k = 170°$. Solid line, PWBA; dotted line, BRM theory; long-dashed line, BH theory; short-dashed line, BR0 theory (for 170° only).

an increase of the cross section, the more so, the closer the photon frequency is to $\omega_{\max}$. Correspondingly, the changes in linear polarization [Fig. 4(b)] increase both with ω and with E_i. For the smaller values of R, P_1 is more negative while for the larger values, P_1 is reduced as compared to the BH results (at energies beyond 20 MeV).

Turning now to the heavier nuclei ^{19}F and ^{89}Y, we show in Fig. 5 the angular dependence of the bremsstrahlung cross sections for 50 MeV electrons and emitted photons of frequency 25 MeV and 40 MeV. The magnetic effects (as considered in the BRM theory) increase the cross sections as they do for protons [Fig. 2(a)]. However, in contrast to the hydrogen nucleus, the PWBA differs from the BH theory already in the forward hemisphere. Moreover, the PWBA leads to cross sections below the ones from the BH theory, the more so, the heavier the nucleus. This is due to the presence of the form factors which can be considerably smaller than unity. Heavy nuclei have a large extension which comes into play at the backward angles that involve high momentum transfers and hence close encounters.

We note that the influence of magnetic and nuclear structure effects on the bremsstrahlung cross sections was already studied by Ginsberg and Pratt [46] within a Born theory that neglects recoil [13]. Their basic results are confirmed by the present calculations: the increase of magnetic and nuclear structure effects both with collision energy and photon angle, the increase of the magnetic effects with ω (at fixed E_i) for backward angles and their independence of ω for small θ_k, as well as the lowering of the cross sections through the form factors for the heavier nuclei.

As concerns the polarization correlations P_1 and P_3 we must keep in mind that in the Bethe-Heitler theory (where the cross section is proportional to Z^2) they are independent of Z and hence the same for all nuclei. In fact, the angular dependence of P_1 for ^{19}F is very similar to the one for ^{1}H [for the parameters of Fig. 2(b)] even when the nuclear structure effects are included. A closer look shows, however, that the increase of P_1 through the inclusion of κ (as compared to the BRM results) which is dominant for ^{1}H, is for ^{19}F counterbalanced by a decrease due to the form factors. As a consequence the BRM and PWBA

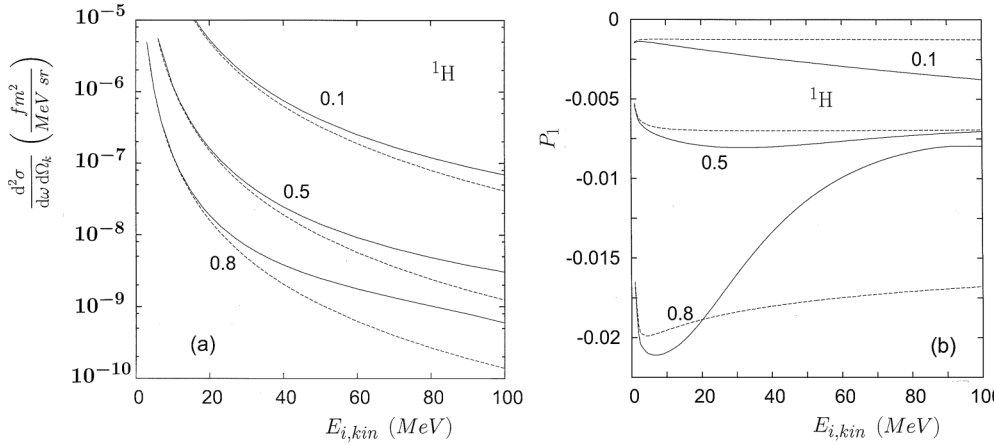

FIG. 4. (a) Doubly differential cross section and (b) linear polarization for $e + p$ collisions as a function of beam energy $E_{i,\text{kin}}$ at photon angle $\theta_k = 170°$. The ratio $R = \omega/E_{i,\text{kin}} = 0.1$ (upper curves), 0.5 (middle curves), 0.8 (lower curves). Solid line, PWBA; long-dashed line, BH theory.

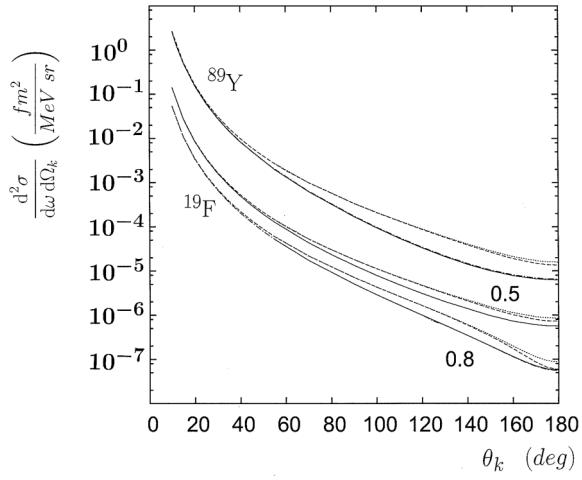

FIG. 5. Doubly differential cross section for 50 MeV electrons colliding with ^{19}F ($Z = 9$; the seven lower curves) and ^{89}Y ($Z = 39$; the four upper curves) as a function of photon angle θ_k. The four lowermost curves are for $\omega = 40$ MeV ($R = \omega/E_{i,\mathrm{kin}} = 0.8$), the other curves are for $\omega = 25$ MeV ($R = 0.5$). Solid line, WPA; dash-dotted line, PWBA (hardly distinguishable from WPA); long-dashed line, BH theory; dotted line, BRM theory.

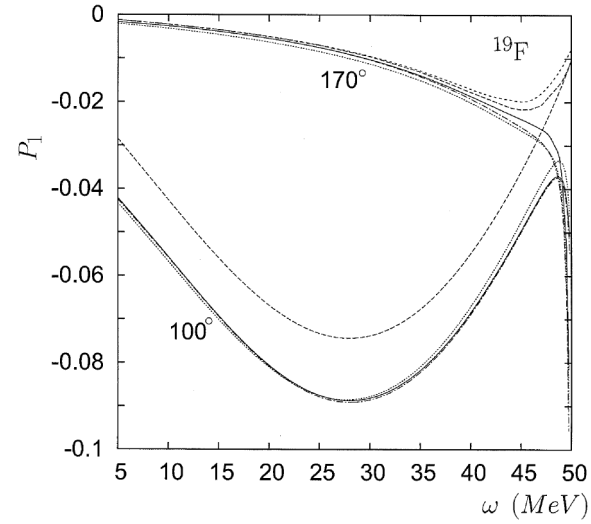

FIG. 7. Linear polarization for 50 MeV $e + {}^{19}$F collisions as a function of photon frequency ω. The lower curves are for photon angle $\theta_k = 100°$, the upper curves are for $\theta_k = 170°$. Solid line, WPA; dash-dotted line, PWBA; dotted line, BRM theory; long-dashed line, BH theory; short-dashed line, SM theory (uppermost curve; for 170° only).

results nearly coincide for all angles in the case of ^{19}F (at 50 MeV and $R = 0.5$). In Fig. 6(a) P_1 is shown at a larger photon energy ($R = 0.8$) where the shape is now different, with an extra shoulder near 60°. The higher-order effects are still tiny, even for the higher energy $E_{i,\mathrm{kin}} = 80$ MeV (and $\omega = 40$ MeV) where the difference between the BRM theory and the PWBA is now quite prominent. Figure 6(b) shows P_1 for ^{89}Y where the basic change with respect to ^{19}F concerns the growing importance of the higher-order effects with increasing nuclear charge. For $Z = 39$ the WPA (see Sec. IV) leads to a noticeable reduction of P_1 as compared to the PWBA at all but the smallest angles. In fact, the WPA results for P_1 agree within 10% for the two nuclei (at equal parameters, 50 MeV and $R = 0.8$) when $\theta_k \lesssim 150°$. If only R is kept fixed but the energy is increased (from 50 to 80 MeV), P_1 gets more negative in a wide angular regime. Not shown in Fig. 6 is, besides the maximum, the minimum of P_1 near zero (which amounts to -0.453 in $\theta_k = 0.36°$ at 80 MeV and $\omega = 40$ MeV as compared to -0.137 in $\theta_k = 0.58°$ at 50 MeV and $\omega = 40$ MeV; note that at such small angles, the BH theory is valid).

In Fig. 7 the frequency dependence of P_1 is shown for ^{19}F at $\theta_k = 100°$ and 170°. As compared to Fig. 3(b), the spectrum extends nearly to ω_{SWL} since the difference between ω_{max} and ω_{SWL} is inversely proportional to M_T [at fixed E_i and θ_k, see Eq. (2.6)]. One should also note that the higher-order effects are visible at the backward angle beyond $\omega = 40$ MeV

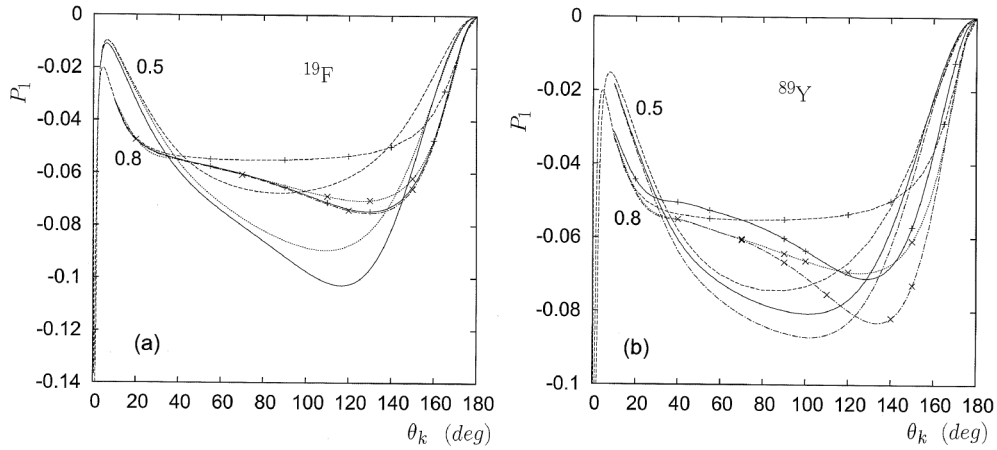

FIG. 6. Angular distribution of the linear polarization for electrons colliding (a) with ^{19}F and (b) with ^{89}Y nuclei. For ^{19}F the photon frequency $\omega = 40$ MeV and the collision energy is 50 MeV ($R = \omega/E_{i,\mathrm{kin}} = 0.8$), respectively 80 MeV ($R = 0.5$). For ^{89}Y the collision energy is 50 MeV and the photon frequency $\omega = 40$ MeV ($R = 0.8$), respectively 25 MeV ($R = 0.5$). Solid line, WPA; dash-dotted line, PWBA; dotted line, BRM theory; long-dashed line, BH theory. The curves for $R = 0.8$ are marked by + (WPA, BH) and × (PWBA, BRM).

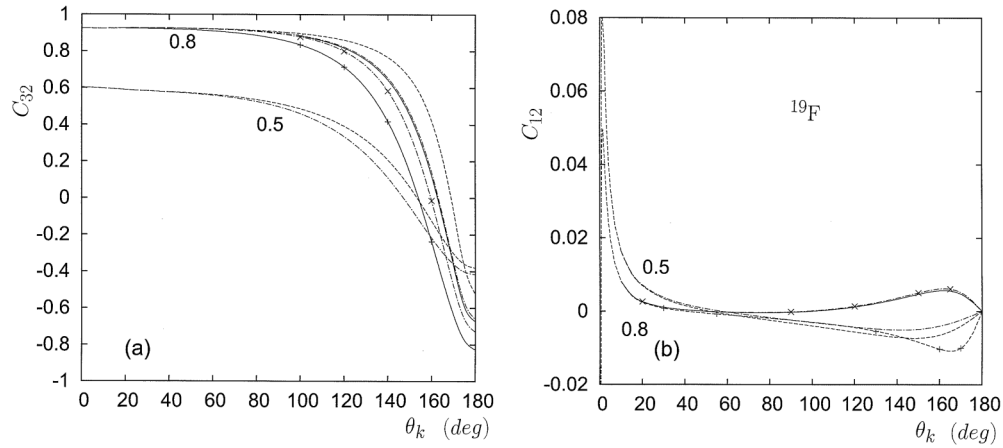

FIG. 8. Angular distribution of the circular polarization correlation P_3 for 50 MeV electrons colliding with ^{19}F and ^{89}Y. (a) For longitudinally spin-polarized electrons (C_{32}) and (b) for transversely (in-plane) spin-polarized electrons (C_{12}). The two bunches of curves are, respectively, for $\omega = 25$ MeV (corresponding to $R = 0.5$) and $\omega = 40$ MeV ($R = 0.8$). Solid line, WPA; dash-dotted line, PWBA; long-dashed line, BH theory. The two curves in (a) marked by + (WPA) and × (PWBA) are the results for ^{89}Y (at $\omega = 40$ MeV). All other results are for ^{19}F. The two curves in (b) marked by + (BH) and × (PWBA) are for $\omega = 40$ MeV.

(i.e., beyond $R = 0.8$) which is in addition illustrated by the comparison between the SM and the BH results. For 100°, the PWBA is valid at all frequencies.

It is important that for bremsstrahlung, due to the presence of the dynamical recoil which increases with Z, the recoil effects do *not* disappear for heavy nuclei (in contrast to elastic electron scattering without radiation). We have tentatively switched off the dynamical recoil (by setting $A_{fi}^{\rm nuc} = 0$) in the BRM model for ^{89}Y. For $E_{i,\rm kin} = 50$ MeV and $\omega = 40$ MeV we have found that for the cross section, the results are similar to those in the BRM theory up to, say, $\theta_k = 120°$, but the deviations increase strongly for larger θ_k(40% reduction at 160°, a factor of 2 at 175° as compared to the BRM results). For P_1, things are even worse, a 10% reduction already at 70° (with a maximum of 80% reduction at 140°–150°).

Now we turn to the circular polarization correlations C_{32} and C_{12} for which, in contrast to P_1, it is necessary that the beam electron is polarized. According to Eq. (2.17), C_{32} is accessible for electrons polarized along the beam direction, i.e., for electrons in a helicity eigenstate. For C_{12}, on the other hand, the electrons have to be polarized transversely to the beam axis, with $\boldsymbol{\zeta}_i$ in the reaction plane. The decrease of C_{32} with photon angle [Fig. 8(a)] from near unity (if ω is near $\omega_{\rm max}$) at $\theta_k = 0$ to negative values close to -1 at $\theta_k = 180°$ is very similar to the one known from lower collision energies [1,17,38]. Also the reduction of the helicity transfer from the electron to the photon at small angles when ω is lowered, combined with a flattening of the angular dependence, is true both at low and high beam energies. For angles beyond 100° and an energy of 50 MeV, the recoil and nuclear structure effects lead to a strong decrease of C_{32}, the more so, the heavier the nucleus. Again, it is seen that higher-order effects are small for ^{19}F, but important for ^{89}Y. In contrast to P_1 [Fig. 6] the onset of the higher-order effects occurs at a much higher angle, and they are most pronounced in the backward hemisphere. In the case of C_{12} [Fig. 8(b)] the nuclear structure effects even produce a change of slope in the angular dependence (as compared to the BH theory) if ω gets close to $\omega_{\rm max}$. Like P_1, also C_{12} has extrema at small angles. For not veiling the large-angle behavior, the minimum is suppressed in the figure (-8.79×10^{-2} at $\omega = 25$ MeV and -5.07×10^{-2} at $\omega = 40$ MeV, both at $\theta_k = 0.25°$).

IV. HIGHER-ORDER THEORY (WPA)

Let us provide an extension of the PWBA which takes the higher-order potential coupling between the electron and the nucleus into account. Since we restrict ourselves to small values of Z/c (the so-called weak-potential approximation) the Sommerfeld-Maue theory can be used for the treatment of the higher-order effects. If recoil and magnetic effects are disregarded, the higher-order contribution $\Delta M_{fi,0}$ to the bremsstrahlung transition operator can be expressed in terms of the difference

$$\Delta M_{fi,0} = M_{fi,0}^{\rm SM} - M_{fi,0}^{\rm BH}. \tag{4.1}$$

The Sommerfeld-Maue transition operator is defined by

$$M_{fi,0}^{\rm SM} = \frac{2\pi^2 c^2}{Z} \int d\boldsymbol{r}\, \chi_{f,\rm SM}^{+}(\boldsymbol{r})(\boldsymbol{\alpha}\boldsymbol{e}_\lambda^*) e^{-i\boldsymbol{k}\boldsymbol{r}} \chi_{i,\rm SM}(\boldsymbol{r}), \tag{4.2}$$

where $\chi_{i,\rm SM}$ and $\chi_{f,\rm SM}$ are the reduced Sommerfeld-Maue wave functions [24,25] (i.e., without electronic four-spinors $u_{k_i}^{(\sigma_i)}$ and $u_{k_{f\infty}}^{(\sigma_f)}$, respectively. For example, the initial electronic state is described by $\psi_i^{(\sigma_i)}(\boldsymbol{r}) = \chi_{i,\rm SM}(\boldsymbol{r}) u_{k_i}^{(\sigma_i)}$ with $\chi_{i,\rm SM}(\boldsymbol{r}) = N_i e^{i\boldsymbol{k}_i\boldsymbol{r}}(1 - \frac{ic}{2E_i}\boldsymbol{\alpha}\boldsymbol{\nabla})_1 F_1(i\eta, 1, i(|\boldsymbol{k}_i|r - \boldsymbol{k}_i\boldsymbol{r}))$, where $N_i = e^{\pi\eta/2}\Gamma(1 - i\eta)(2\pi)^{-3/2}$, $\eta = ZE_i/(|\boldsymbol{k}_i|c^2)$ and ${}_1F_1$ a confluent hypergeometric function). Upon neglecting the term quadratic in $\boldsymbol{\alpha}\boldsymbol{\nabla}$ [which is of order $(Z/c)^2$], Eq. (4.2) can be evaluated analytically as, e.g., given in [23,25,35].[3]

[3]In [35], the first term in (A.3) should read $[1 + c\boldsymbol{\alpha}\boldsymbol{p}_0/2E_f']\boldsymbol{\alpha}\boldsymbol{I}_0$.

$M^{\rm BH}_{fi,0}$ is the first-order Born (Bethe-Heitler) transition operator [2,19],

$$M^{\rm BH}_{fi,0} = \frac{1}{q^2_\infty}\left\{\boldsymbol{\alpha}\boldsymbol{e}^*_\lambda \frac{\boldsymbol{\alpha}c(\boldsymbol{k}_{f\infty}+\boldsymbol{k})+\beta c^2+E_i}{(\boldsymbol{k}_{f\infty}+\boldsymbol{k})^2-\boldsymbol{k}_i^2} + \frac{\boldsymbol{\alpha}c(\boldsymbol{k}_i-\boldsymbol{k})+\beta c^2+E_{f\infty}}{(\boldsymbol{k}_i-\boldsymbol{k})^2-\boldsymbol{k}^2_{f\infty}}\boldsymbol{\alpha}\boldsymbol{e}^*_\lambda\right\}. \quad (4.3)$$

This expression derives from the electronic transition operator in Eq. (2.1) if the magnetic scattering is disregarded (i.e., only $\nu = 0$ is retained) and if, in addition, $M_T \to \infty$ (i.e., if recoil is neglected) such that E_f is replaced by $E_{f\infty} = \sqrt{\boldsymbol{k}^2_{f\infty}c^2+c^4} = E_i - \omega$ and consequently $-q^2$ is replaced by $\boldsymbol{q}^2_\infty \equiv (\boldsymbol{k}_i - \boldsymbol{k}_{f\infty} - \boldsymbol{k})^2$.

If the modifications arising from recoil and magnetic scattering (quantified by the difference between the BRM and the BH results) are moderate, say, below 20%, the higher-order perturbation of the $\nu \geqslant 1$ terms and of $A^{\rm nuc}_{fi}$ may be neglected. It will then be sufficient just to include Eq. (4.1) in the potential scattering ($\nu = 0$) contribution to the electron bremsstrahlung matrix element. In this approximation, termed WPA, the cross section is calculated from Eq. (2.9) with $A^{\rm el}_{fi} + A^{\rm nuc}_{fi}$ replaced by $A^{\rm el}_{fi} + \Delta A_{fi,0} + A^{\rm nuc}_{fi}$, where

$$\Delta A_{fi,0} = \left(u^{(\sigma_f)+}_{k_f}\Delta M_{fi,0}u^{(\sigma_i)}_{k_i}\right)\frac{Z}{2\pi^2c^2}\left(U^{(s_f)+}_{P_f}\gamma_0\Gamma_0(q)U^{(s_i)}_{P_i}\right). \quad (4.4)$$

In this theory the linearity of the transition amplitude in the form factors is retained. This may be justified by considering the second-order Born amplitude (see, e.g., [2,22]). From Eq. (3.1) it follows that the Fourier transform $V(q)$ of the nuclear potential, generated by $\varrho(r)$, factorizes according to $V(q) = V_0(q)\cdot G_E(q)$ where V_0 corresponds to a point-like nucleus. Hence the form factors enter into the second-order Born amplitude as products $G_E(k_i - k - p)\cdot G_E(p - k_f)$ where p is an integration variable. Taken into consideration that the corresponding integrand is peaked both for $p = k_f$ and for $p = k_i - k$, it follows that one is approximately left with a linear dependence on $G_E(k_i - k - k_f) = G_E(q)$ since $G_E(0) = 1$. Whereas for elastic electron scattering such an approximation fails near the zeros of $G_E(q)$, the additional integral over the electronic degrees of freedom in the bremsstrahlung case implies an average over a range of momentum transfers such that the above-mentioned peaking approximation will be less severe. This averaging is the more effective the larger the final energy of the electron.

V. RESULTS FOR THE POLARIZATION CORRELATIONS P_2 AND A

For the numerical evaluation of the WPA we recall some important properties of the Sommerfeld-Maue transition operator $M^{\rm SM}_{fi,0}$ in Eq. (4.2). As explicitly formulated in [35], it is determined by four parameters, $\tilde\alpha$, $\tilde\beta$, $\tilde\gamma$, $\tilde\delta$, which are quadratic functions of the electron and photon momenta. It has complex first-order poles (plus branch cuts) at $\tilde\gamma = 0$ and at $\tilde\alpha + \tilde\beta = 0$ (i.e., when $z \equiv \frac{\tilde\alpha\tilde\delta - \tilde\beta\tilde\gamma}{\tilde\alpha(\tilde\gamma+\tilde\delta)} = 1$), which appear near $\vartheta_f = \theta_k$ and $\varphi_f = 0$ (where ϑ_f and φ_f are, respectively, the polar and azimuthal angles of $\boldsymbol{k}_f$). These poles approach the real axis when $E_i \to \infty$ but, because of the finite electron mass, the transition operator and hence the corresponding integrand in Eq. (2.9) is never singular. Due to the semirelativistic nature of the Sommerfeld-Maue functions the poles agree with those of the Bethe-Heitler transition operator (4.3) rather than with those of the recoil-modified amplitudes (2.2). Therefore one cannot account for the kinematical recoil in the SM theory by merely replacing $|\boldsymbol{k}_{f,\infty}|$ with $|\boldsymbol{k}_f|$. If one introduces in addition modified parameters such that the zeros of the modified $\tilde\gamma$ and $\tilde\alpha + \tilde\beta$ agree with the poles of Eq. (2.2) (which can be achieved by changing $\tilde\gamma$ to $-((\boldsymbol{k}_f+\boldsymbol{k})^2 - (\frac{(E_f+\omega)^2}{c^2} - c^2))/2 + i\epsilon$ and $\tilde\beta$ to $(\boldsymbol{k}_i - \boldsymbol{k})\boldsymbol{k}_f - \boldsymbol{k}_f^2/2 - (\frac{(E_i-\omega)^2}{c^2} - c^2)/2 - i\epsilon$ with $\epsilon = +0$), a quite good account of the kinematical recoil for the heavier nuclei can be obtained. However, taken into consideration that hydrogen does not require a higher-order theory and that for ^{19}F or heavier nuclei kinematical recoil effects are at most in the percent region, the WPA as formulated in Sec. IV is sufficiently accurate in this respect.

The applicability of the WPA, as measured in terms of the deviations between the BH and the BRM models, is governed by similar criteria as those which control the smallness of the higher-order effects. This is related to the fact that the contribution of recoil and magnetic scattering to the bremsstrahlung cross section, while being small in the forward hemisphere, also increases with photon frequency and angle. However, instead of the nuclear charge, the decisive parameters are now the beam energy besides the fraction $R = \omega/E_{i,\rm kin}$. Thus, both for ^{19}F and ^{89}Y, the deviations between the BH and the BRM cross section results are 15–20% for 50 MeV and $R = 0.5$ in the worst case ($\theta_k = 180^\circ$), while they will exceed 20% for $\theta_k \gtrsim 160^\circ$ if $R = 0.8$, but even if $R = 0.5$ when the beam energy is increased to 80 MeV.

The linear polarization correlation P_2 and the spin asymmetry A are only accessible by the WPA since they vanish in the first-order Born approximation [1,22] and hence in the PWBA. Accordingly, their moduli are much smaller than those of P_1 or P_3 as long as Z/c (i.e., the higher-order effect) is small. It follows from Fig. 9 (in comparison with Figs. 6 and 8) that for the two nuclei considered, ^{19}F and ^{89}Y, the respective reduction is between one and three orders of magnitude in the backward hemisphere. In the figure, comparison is made with the SM theory to display the recoil and nuclear structure effects. In contrast to P_1 or P_3, the onset of these effects is already at forward angles. For $P_2(0)$, corresponding to electrons spin-polarized along the beam direction [Fig. 9(a)], the SM theory becomes invalid for ^{89}Y if $\theta_k \gtrsim 20^\circ$. While the SM theory predicts a negative value at all angles, the WPA leads to a positive $P_2(0)$ beyond 50°–70°. The change of the angular distribution by the relativistic nuclear effects is even more striking in the case of transversely spin-polarized electrons [Fig. 9(b)], where the decrease of $P_2(90^\circ)$ with angle continues beyond 5° whereas the SM theory predicts an increase of the polarization correlation in the angular region 5°–30° for both targets.

The spin asymmetry A, relating to electrons spin-polarized perpendicular to the plane spanned by $\boldsymbol{k}_i$ and $\boldsymbol{k}$, is independent of the photon polarization. For Z/c small, A increases linearly

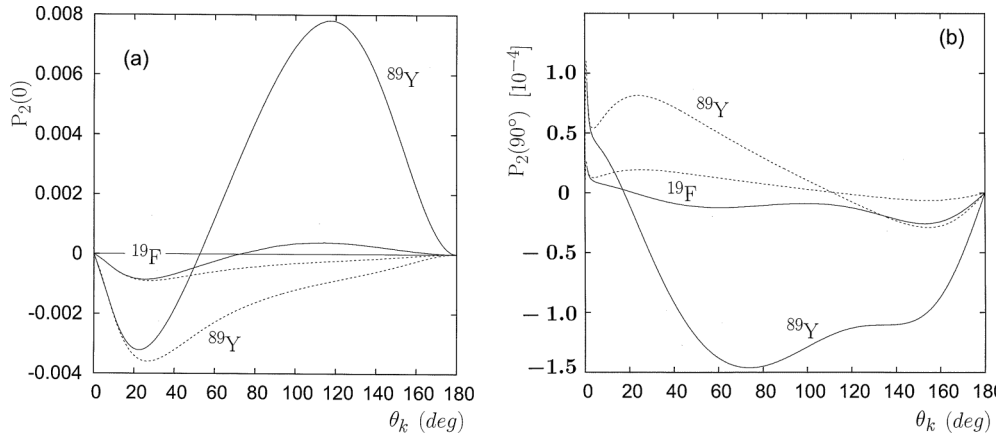

FIG. 9. Angular distribution of the linear polarization correlation P_2 for 50 MeV electrons colliding with ^{19}F and ^{89}Y. The photon frequency is $\omega = 25$ MeV. (a) For longitudinally spin-polarized electrons [$P_2(0)$] and (b) for transversely (in-plane) spin-polarized electrons [$P_2(90°)$]. Solid line, WPA; short-dashed line, SM theory.

with Z and has a pronounced peak in the backward hemisphere (which moves to the back-most angles when ω approaches $\omega_{\max}$ [37,38]). The consideration of recoil and nuclear structure effects leads to a significant reduction of the spin asymmetry at large θ_k. When the collision energy is increased (but R and θ_k kept fixed), A decreases strongly (even more in WPA than in the SM theory) which is shown for ^{19}F in Fig. 10(a) by comparing the results for collision energies 50 MeV and 80 MeV at $R = 0.5$. Not shown in the figure is a small minimum of A at angles close to zero (where the SM theory is valid). As known from investigations at lower energy [37] this minimum depends on the ratio R and develops into a broad minimum at much higher angles when $\omega \to \omega_{\max}$. Keeping $R = 0.5$ fixed, the minimum of A is -1.81×10^{-5} at $\theta_k = 0.5°$ for 50 MeV $e + ^{19}$F, but is less pronounced for the higher collision energy (-7.86×10^{-6} at 0.3° for 80 MeV). In contrast, for the heaviest nucleus ^{89}Y the minimum is much deeper than for ^{19}F (-7.74×10^{-5} at 0.5° for 50 MeV $e + ^{89}$Y and $R = 0.5$), but still small as compared to the backward maximum. Figure 10(b) displays the strong increase of A when $\omega \to \omega_{\max}$ which holds true for all angles in the backward hemisphere. At small ω and large angles this feature is even enhanced by the recoil and nuclear structure effects. The increase with ω at the backward angles when ω approaches the high-energy end of the spectrum is, albeit less than for A, common to all polarization correlations. It mirrors the fact that polarization asymmetries are highly relativistic effects which are enhanced at large momentum transfers.

VI. CONCLUSION

We have investigated the high-energy behavior of the bremsstrahlung intensity and polarization correlations within the plane-wave Born approximation and the higher-order weak potential approximation, taking into account the relativistic nuclear effects which comprise the recoil of the nucleus, the magnetic scattering as well as the nuclear structure effects in

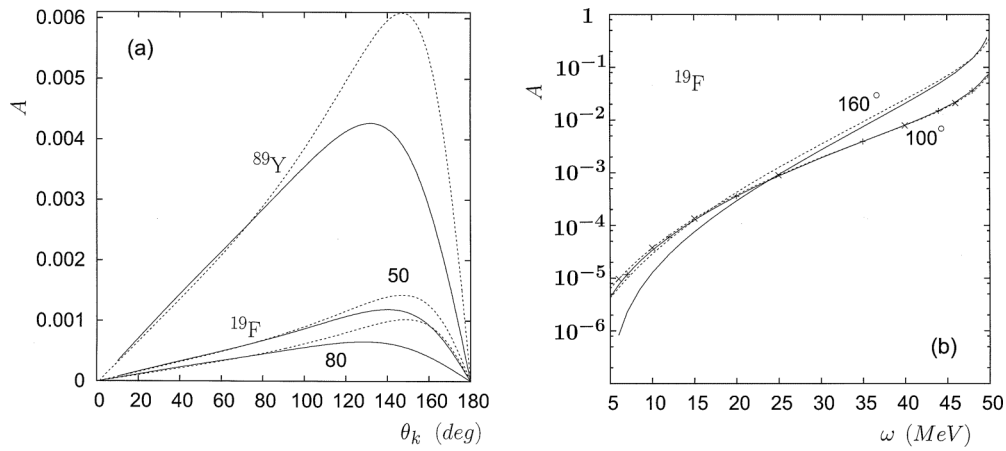

FIG. 10. Spin asymmetry A for electrons spin-polarized perpendicular to the reaction plane colliding with ^{19}F and ^{89}Y nuclei. (a) As a function of photon angle θ_k for ^{89}Y with $E_{i,\mathrm{kin}} = 50$ MeV and $\omega = 25$ MeV (uppermost curves), as well as for ^{19}F at $E_{i,\mathrm{kin}} = 50$ MeV and $\omega = 25$ MeV (middle curves) and at $E_{i,\mathrm{kin}} = 80$ MeV and $\omega = 40$ MeV (lowermost curves). (b) As a function of photon frequency ω for 50 MeV $e + ^{19}$F collisions at $\theta_k = 100°$ and 160°. Solid line, WPA; short-dashed line, SM theory. The results for $\theta_k = 100°$ are marked with + (WPA) and × (SM).

terms of form factors and the anomalous magnetic moment. Due to the averaging procedure over a finite range of momentum transfers, inherent in the summation over the unobserved final states of the scattered electron, the validity of the WPA, as controlled by the smallness of both the higher-order effects and the recoil and magnetic scattering effects, extends to considerably higher nuclear charges Z than is the case for elastic electron scattering. Thus, in our examples, we could cover the range $1 \leqslant Z < 40$. The necessary restrictions, such as avoiding photon frequencies too close to the high-energy end of the spectrum for backward photon emission, guarantee the correctness of the WPA cross sections as well as of those polarization correlations (P_1, P_3) which do not vanish in the PWBA. However, the WPA estimates for the linear polarization P_2 and the spin asymmetry A at beam energies near 50 MeV and beyond might suffer from inaccuracies, particularly for the ^{89}Y nucleus.

In accord with early cross section results on high-energy bremsstrahlung [46], we have found that the relativistic nuclear effects increase with photon angle θ_k, with photon frequency ω (at large angles) and with collision energy $E_{i,\mathrm{kin}}$. In particular, for protons and energies up to 100 MeV the photon intensity increases with angle in the backward hemisphere relative to the Bethe-Heitler theory, because of the magnetic scattering. For the heavier and more extended nuclei, there is a strong reduction of the cross section from the additional influence of the form factors.

The conjecture, put forth in the literature, that recoil is negligible could only be confirmed for very small photon angles. In contrast, for wide-angle bremsstrahlung this is no longer true. Because of the presence of the dynamical recoil which behaves like qZ/M_Tc, recoil is nearly equally important for heavy nuclei as it is for protons. In most cases the *cross section* results are not qualitatively changed by the consideration of recoil (if magnetic scattering is included). An exception is the reduction of the high-energy end of the spectrum by the kinematical recoil, the more so (being a q/M_Tc effect), the larger θ_k, the higher the beam energy and the lighter the nucleus. Consequently, the cross section drops rapidly below the BH result when the maximum frequency is reached.

Turning to the polarization correlations we have verified that the dependence of their angular distribution on collision energy and photon frequency, established earlier for fixed point nuclei, remains in general valid up to beam energies of 10–20 MeV. At higher energies the perturbation due to recoil, magnetic scattering and nuclear structure effects leads to noticeable modifications which are in general much stronger than for the cross sections. These modifications are again most prominent at the backward photon angles and at high frequencies which are associated with a large momentum transfer to the nucleus, respectively with small electron-nucleus distances.

The linear polarization P_1, being most easily accessible to experiment because a polarized electron beam is not required, is studied in greatest detail. In the Bethe-Heitler theory the angular distribution of P_1 is independent of the target (at fixed ω and $E_{i,\mathrm{kin}}$). This is no longer true when the relativistic nuclear effects are accounted for, although the angular dependence remains mostly similar for the different targets. In particular we have found that for a fixed backward angle P_1 decreases strongly with photon frequency for all targets, due to the dynamical recoil and the magnetic scattering. This is to be contrasted to the increase of P_1 with ω in the BH theory near the short-wavelength limit.

A particular object in view, investigated in many low-energy experiments, is the spin asymmetry A. Relating to an electron spin-polarized perpendicular to the reaction plane it is extremely sensitive to relativistic effects which are strong for heavy nuclei at short electron-nucleus distances and hence lead to large spin asymmetries. Characteristic of A is the large maximum at angles near or beyond 140°. Moreover, A grows strongly (by several orders of magnitude) when, at fixed $E_{i,\mathrm{kin}}$, ω is increased to the high-energy end of the spectrum. While the increase of A with ω is not notably changed when the relativistic nuclear effects are taken into consideration, the maximum of A is considerably reduced, the more so, the higher the collision energy. A similar reduction of the spin asymmetry by the nuclear structure effects is known from elastic electron scattering [34,47]. This similarity is, however, only true for electrons spin-polarized perpendicular to the scattering plane. For longitudinally spin-polarized electrons, for example, helicity transfer (measured by C_{32} in bremsstrahlung) is reduced at the backward angles, the more so, the heavier the nucleus and the higher ω. For elastic electron scattering the helicity transfer is *enhanced* by the nuclear structure effects. This behavior contradicts the results for heavy point nuclei where the respective polarization correlations agree at ultrahigh collision energies [38]. Experiments on high-energy bremsstrahlung are highly welcome.

[1] H. K. Tseng and R. H. Pratt, Phys. Rev. A **7**, 1502 (1973).
[2] E. Haug and W. Nakel, *The Elementary Process of Bremsstrahlung* (World Scientific, Singapore, 2004), pp. 32, 147; 107.
[3] S. Tashenov *et al.*, Phys. Rev. Lett. **97**, 223202 (2006).
[4] S. Tashenov, T. Bäck, R. Barday, B. Cederwall, J. Enders, A. Khaplanov, Yu. Poltoratska, K.-U. Schässburger, and A. Surzhykov, Phys. Rev. Lett. **107**, 173201 (2011).
[5] R. Barday, K. Aulenbacher, P. Bangert, J. Enders, A. Göök, D. H. Jakubassa-Amundsen, F. Nillius, A. Surzhykov, and V. A. Yerokhin, J. Phys.: Conf. Series **298**, 133 (2010).
[6] F. Nillius and K. Aulenbacher, in Ref. [5], p. 147.
[7] R. Märtin *et al.*, Phys. Rev. Lett. **108**, 264801 (2012).
[8] J. Goldemberg and R. H. Pratt, Rev. Mod. Phys. **38**, 311 (1966).
[9] M. Greco, A. Tenore, and A. Verganelakis, Phys. Lett. B **27**, 317 (1968).
[10] L. I. Schiff, Phys. Rev. **87**, 750 (1952).
[11] N. Meister and D. R. Yennie, Phys. Rev. **130**, 1210 (1963).
[12] L. C. Maximon and D. B. Isabelle, Phys. Rev. **133**, B1344 (1964).
[13] E. S. Ginsberg and R. H. Pratt, Phys. Rev. **134**, B773 (1964).
[14] S. Tashenov, Nucl. Instrum. Methods Phys. Res. A **640**, 164 (2011).
[15] S. Tashenov *et al.*, Phys. Rev. A **87**, 022707 (2013).

[16] H. K. Tseng and R. H. Pratt, Phys. Rev. A **19**, 1525 (1979).
[17] V. A. Yerokhin and A. Surzhykov, Phys. Rev. A **82**, 062702 (2010).
[18] E. Haug, Eur. Phys. J. D **58**, 297 (2010).
[19] H. Bethe and W. Heitler, Proc. R. Soc. London A **146**, 83 (1934).
[20] C. Kacser, Proc. R. Soc. London A **253**, 103 (1959).
[21] W. R. Johnson and J. D. Rozics, Phys. Rev. **128**, 192 (1962).
[22] E. S. Sobolak and P. Stehle, Phys. Rev. **129**, 403 (1963).
[23] G. Elwert and E. Haug, Phys. Rev. **183**, 90 (1969).
[24] A. Sommerfeld and A. W. Maue, Ann. Phys. (Leipzig) **22**, 629 (1935).
[25] H. A. Bethe and L. C. Maximon, Phys. Rev. **93**, 768 (1954).
[26] S. D. Drell, Phys. Rev. **87**, 753 (1952).
[27] E. A. Allton and E. F. Erickson, Phys. Rev. D **3**, 762 (1971).
[28] S. J. Biel and E. H. S. Burhop, Proc. Phys. Soc. London A **68**, 165 (1955).
[29] R. A. Berg and C. N. Lindner, Phys. Rev. **112**, 2072 (1958).
[30] L. C. Maximon and D. B. Isabelle, Phys. Rev. **136**, B674 (1964).
[31] A. I. Achieser and W. B. Berestezki, *Quantenelelectrodynamik* (Teubner, Wiesbaden, 1962), Chap. 29.10.
[32] J. D. Bjorken and S. D. Drell, *Relativistic Quantum Mechanics* (McGraw-Hill, New York, 1964), Chaps. 7.6 and 10.9.
[33] F. Gross, *Relativistic Quantum Mechanics and Field Theory* (Wiley, New York, 1993), pp. 294, 596.
[34] D. H. Jakubassa-Amundsen, Nucl. Phys. A **896**, 59 (2012).
[35] D. H. Jakubassa-Amundsen, J. Phys. B **40**, 2719 (2007).
[36] K. Blum, *Density Matrix Theory and Applications* 2nd ed. (Plenum Press, New York, 1996), Chap. 1.2.5.
[37] D. H. Jakubassa-Amundsen, Phys. Rev. A **82**, 042714 (2010).
[38] D. H. Jakubassa-Amundsen, Phys. Rev. A **85**, 042714 (2012).
[39] T. W. Donnelly and I. Sick, Rev. Mod. Phys. **56**, 461 (1984).
[40] R. Hofstadter, F. Bumiller, and M. R. Yearian, Rev. Mod. Phys. **30**, 482 (1958).
[41] H. De Vries, C. W. De Jager, and C. De Vries, At. Data Nucl. Data Tables **36**, 495 (1987).
[42] W. M. Haynes, *CRC Handbook of Chemistry and Physics*, 91st ed. (Taylor and Francis Group, Boca Raton, FL, 2010), Chap. 11.
[43] R. H. Pratt, J. D. Walecka, and T. A. Griffy, Nucl. Phys. **64**, 677 (1965).
[44] J. E. Wise *et al.*, Phys. Rev. C **47**, 2539 (1993).
[45] H. Olsen and L. C. Maximon, Phys. Rev. **114**, 887 (1959).
[46] E. S. Ginsberg and R. H. Pratt, Phys. Rev. **137**, B1500 (1965).
[47] P. Uginčius, H.Überall, and G. H. Rawitscher, Nucl. Phys. A **158**, 418 (1970).